Table 1. Baseline characteristics of the patients

	All (n = 122)	SVR (n = 63)	TR (n = 14)	NVR (n = 45)
Males/females	54/68	31/32	6/8	17/28
Age, years	61 (20–78)	62 (20–78)	60.5 (47–75)	59 (36–75)
BMI	22.9 (15.2–29.1)	22.2 (15.2–27.3)	24.55 (18.4–29.0)	23.5 (18.1–29.1)
Fibrosis (0–2/3–4)	66/18	36/4	9/2	21/12
Activity (0–1/2–3)	33/51	17/23	7/4	9/24
ISDR (0, 1/≥2)	30/18	9/9	4/2	17/7
aa70 (wild type/mutant)	26/19	12/4	5/1	9/14
aa91 (wild type/mutant)	29/19	12/4	4/2	13/13
WBC, /l	4.6×10^9 (1.4×10^9–8.1×10^9)	4.8×10^9 (2.1×10^9–7.8×10^9)	4.6×10^9 (3.0×10^9–6.0×10^9)	4.4×10^9 (1.4×10^9–8.1×10^9)
Hemoglobin, g/dl	13.6 (9.7–17.6)	13.7 (10.7–16.6)	13.75 (10.8–17.1)	13.2 (9.7–17.6)
Platelets, $\times 10^{-4}$/l	15.3×10^6 (4.0×10^6–39.8×10^6)	16.7×10^6 (4.0×10^6–39.8×10^6)	17.15×10^6 (6.8×10^6–27.1×10^6)	13.0×10^6 (5.5×10^6–30×10^6)
AST, IU/l	48 (17–146)	43 (18–138)	36 (17–123)	64.0 (20–146)
ALT, IU/l	49.5 (13–218)	39 (15–182)	42 (13–218)	57 (18–199)
γGTP, IU/l	32.5 (10–326)	30 (10–297)	29 (14–326)	43 (15–317)
Albumin, g/dl	4.2 (3.1–4.9)	4.3 (3.4–4.8)	4.2 (3.7–4.6)	4.0 (3.1–4.9)
Total cholesterol, mg/dl	168 (117–240)	176 (119–240)	167 (134–239)	160 (117–235)
Viral load	2,300 (103–40,000)	2,100 (110–40,000)	4,900 (500–25,000)	2,200 (103–22,000)
PEG-IFN-α2b, μg	80 (60–140)	80 (60–140)	90 (60–120)	80 (60–120)
PEG-IFN-α2b/kg/week, μg/kg/week	1.37 (0.31–1.95)	1.42 (0.31–1.95)	1.40 (0.71–1.59)	1.16 (0.51–1.66)
Ribavirin, mg	600 (400–800)	600 (400–800)	600 (400–800)	600 (400–800)
Ribavirin/kg/day, mg/kg/day	10.1 (2.85–15.59)	10.22 (4.21–15.59)	9.52 (4.48–12.9)	9.76 (2.85–12.94)
rs8099917 (TT/non-TT)	78/44	53/10	9/5	16/29

For categorical data, the number of patients in each category is shown. For continuous data, the median and range are displayed.

ALT = Alanine aminotransferase; AST = aspartate aminotransferase; BMI = body mass index; γGTP = γ-glutamyl transpeptidase; NVR = non-virological response; TR = transient response; WBC = white blood cells.

Table 2. Predictive factors for SVR using univariate analysis

	SVR (n = 63)	TR+NVR (n = 59)	p
Males/females	31/32	23/36	0.278
Age, years	62 (20–78)	59 (36–75)	0.216
BMI	22.2 (15.2–27.3)	23.7 (18.1–29.1)	0.005
Fibrosis (0–2/3–4)	36/4	30/14	0.149
Activity (0–1/2–3)	17/23	16/28	0.656
ISDR (0, 1/2≥)	9/9	21/9	0.222
aa70 (wild type/mutant)	12/4	14/15	0.118
aa91 (wild type/mutant)	12/4	17/15	0.212
WBC, /l	4.8×10^9 (2.1×10^9–7.8×10^9)	4.5×10^9 (1.4×10^9–8.1×10^9)	0.232
Hemoglobin, g/dl	13.7 (10.7–16.6)	13.4 (9.7–17.6)	0.418
Platelets, $\times 10^{-4}$/l	16.7×10^6 (4.0×10^6–39.8×10^6)	14.5×10^6 (5.5×10^6–30×10^6)	0.054
ALT, IU/l	39 (15–182)	54 (13–218)	0.055
γGTP, IU/l	30 (10–297)	34 (14–326)	0.072
Albumin, g/dl	4.3 (3.4–4.8)	4.1 (3.1–4.9)	0.018
Total cholesterol, mg/dl	176 (119–240)	161 (117–239)	0.018
Viral load	2,100 (110–40,000)	2,640 (103–25,000)	0.396
PEG-IFN-α2b, μg	80 (60–140)	80 (60–120)	0.184
PEG-IFN-α2b/kg/week, μg/kg/week	1.42 (0.31–1.95)	1.18 (0.51–1.66)	<0.001
Ribavirin, mg	600 (400–800)	600 (600–800)	0.196
Ribavirin/kg/day, mg/kg/day	10.22 (4.21–15.59)	9.76 (2.8–12.9)	0.014
rs8099917 (TT/non-TT)	53/10	25/34	<0.001

For categorical data, the number of patients in each category is shown. For continuous data, the median and range are displayed.

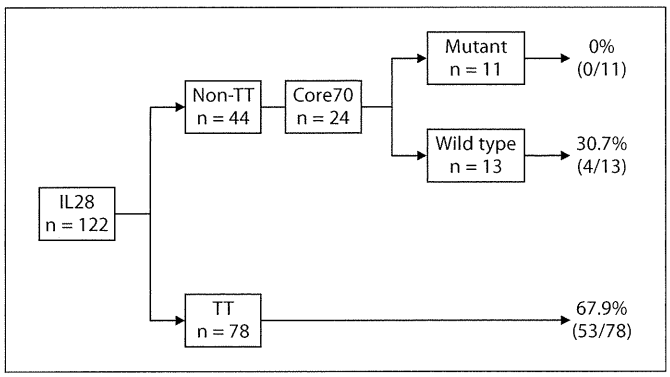

Fig. 2. Predicting SVR by core70 in combination with the IL28B genotype. SVR was achieved by 67.9% of patients with the rs8099917 genotype TT. Among the patients with the rs8099917 genotype TT, those with core70 wild type achieved a high rate of SVR (30.7%), and the SVR rate was worst in patients with core 70 mutant type (0%).

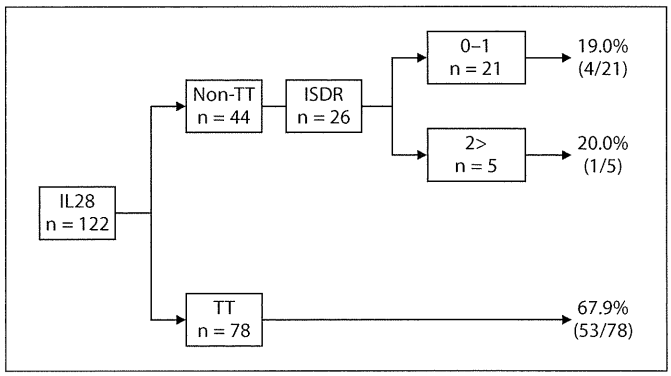

Fig. 3. Predicting SVR by ISDR in combination with the IL28B genotype. Among patients with the rs8099917 genotype TT, the SVR rate did not differ between ISDR wild type (20%) and ISDR mutant type (19.0%).

2.278–24.257, p = 0.001) and PEG-IFN dose (odds ratio 7.162, 95% CI 1.565–18.15, p = 0.007) were significant factors (table 3).

Relationship between PEG-IFN Dose and the rs8099917 Genotype

We evaluated the relationship between the cumulative PEG-IFN dose and the rs8099917 genotype (fig. 1). The cumulative PEG-IFN dose was classified as <60%, 60–80% and >80%. Among the patients with <60% of the PEG-IFN dose, SVR was achieved by 30.8% (4 of 13 patients), 20.0% (1 of 5 patients) and 27.8% (5 of 18 patients) of patients with genotype TT, non-TT and in total, respectively. Among the patients with 60–80% of PEG-IFN dose, SVR was achieved by 22.2% (2 of 9 patients), 0.0% (0 of 16 patients) and 8.0% (2 of 25 patients) of patients with genotype TT, non-TT and in total, respectively. Finally, among the patients with >80% of PEG-IFN dose, SVR was achieved by 83.9% (47 of 56 patients), 39.1% (9 of 23 patients) and 70.9% (56 of 79 patients) of patients with genotype TT, non-TT and in total, respectively.

Virological Response according to the rs8099917 Genotype, Core aa70 and ISDR

The SVR rates according to the rs8099917 genotype and core aa70 are shown in figure 2. Among patients with the rs8099917 genotype TT, SVR was achieved by 67.9% (53 of 78 patients). Among patients with the rs8099917 genotype non-TT, a marginally higher proportion of patients with core 70 wild type (30.7%) achieved SVR than did patients with core 70 mutant type (0%; p = 0.1323).

Table 3. Predictive factors for SVR using multivariate analysis (logistic regression model)

	Odds ratio	95% CI	p value
rs8099917 (TT/non-TT)	7.434	2.278–24.257	0.001
PEG-IFN dose (1.37 μg/kg/week)	7.162	1.565–18.15	0.007

The SVR rates according to the rs8099917 genotype and ISDR are shown in figure 3. Among patients with the rs8099917 genotype non-TT, the SVR rate did not differ between ISDR wild type (20%) and ISDR mutant type (19.0%; p = 1).

Discussion

In this study, we showed by multivariate analysis that the rs8099917 genotype and total PEG-IFN dose contribute to the successful outcome of PEG-IFN plus ribavirin combination treatment for infection with HCV genotype 1.

Several host and viral factors contribute to SVR in PEG-IFN plus ribavirin combination treatment of Japanese patients infected with HCV genotype 1 and who have high viral loads. The host factors include younger age, male gender, mild liver fibrosis, platelet count, LDL cholesterol values and γ-glutamyl transpeptidase values.

Recent reports have shown that the rs8099917 genotype was a pretreatment predictor of virological response to 48-week PEG-IFN plus ribavirin combination treatment for infection with HCV genotype 1 [11–13]. The present study revealed that the rs8099917 genotype was a significant factor for prediction of SVR (odds ratio 6.159, 95% CI 1.326–28.618, p = 0.02). The cumulative doses of PEG-IFN and ribavirin also were important factors that affected the treatment outcome [15–18]. This study revealed that the total dose of PEG-IFN was a significant factor for prediction for SVR (odds ratio 6.398, 95% CI 1.527–26.8, p = 0.011). For the rs8099917 genotype TT, SVR rates of patients given doses <60% and 60–80% of PEG-IFN were low (30.8 and 40%), and this was so even in those given >80% of PEG-IFN (71%). This result indicates that a dose of PEG-IFN above 80% is necessary for SVR in patients with the rs8099917 genotype TT. In addition, for the rs8099917 genotype non-TT, the SVR rates of patients given doses <60% and 60–80% of PEG-IFN were low (20 and 0%), and this was so even in those given >80% of PEG-IFN (40.0%). This result indicates that a dose of PEG-IFN above 80% is necessary for SVR in patients with the rs8099917 genotype non-TT as well.

A number of studies have reported a significant association between HCV core70/core91 substitutions and treatment outcome [8, 15, 16]. However, in this study, we found no such association but the numbers of patients who were tested for HCV core70/core91 mutations may have been too few. The ISDR located in the NS5A region was originally reported in 1996 by Enomoto et al. [14] and confirmed by several Asian studies [19–21]. This study did not find a significant association between the ISDR and SVR. In addition, controversial results have been reported from Western studies [22, 23].

This study indicated the value of a combination of the rs8099917 genotype and core70 substitutions for prediction of SVR. The patients with the rs8099917 genotype TT had high rates of SVR (67.9%). SVR was achieved by 30.7% of patients with the rs8099917 genotype non-TT and core 70 wild type. The SVR rate was worst in patients with the rs8099917 genotype non-TT and core 70 mutant type. These results indicate the effects of both host and viral factors on IFN responsiveness. However, a combination of the IL28 genotype and ISDR substitutions for prediction of SVR was not useful. Thus, in patients with the rs8099917 genotype non-TT, SVR rates did not differ between ISDR wild type (20%) and ISDR mutant type (19.0%).

In conclusion, the rs8099917 genotype and total PEG-IFN dose were associated with response to IFN in patients with HCV genotype 1. A combination of host and viral factors could improve prediction of the IFN response.

Disclosure Statement

The authors have no conflict of interest to declare.

References

1 Global Burden of Hepatitis C Working Group: Global burden of disease (GBD) for hepatitis C. J Clin Pharmacol 2004;44:20–29.

2 Barrera JM, Bruguera M, Ercilla MG, Gil C, Celis R, Gil MP, del Valle Onorato M, Rodés J, Ordinas A: Persistent hepatitis C viremia after acute self-limiting postttransfusion hepatitis. Hepatology 1995;21:639–644.

3 Niederau C, Lange S, Heintges T, Erhardt A, Buschkamp M, Hürter D, Nawrocki M, Kruska L, Hensel F, Petry W, Häussinger D: Prognosis of chronic hepatitis C: results of a large, prospective cohort study. Hepatology 1998;28:1687–1695.

4 Kiyosawa K, Sodeyama T, Tanaka E, Gibo Y, Yoshizawa K, Nakano Y, Furuta S, Akahane Y, Nishioka K, Purcell RH, et al: Inter-relationship of blood-transfusion, non-A, non-B hepatitis and hepatocellular carcinoma – analysis by detection of antibody to hepatitis-C virus. Hepatology 1990;12:671–675.

5 Manns MP, McHutchison JG, Gordon SC, Rustgi VK, Shiffman M, Reindollar R, Goodman ZD, Koury K, Ling M, Albrecht JK: Peginterferon alfa-2b plus ribavirin compared with interferon alfa-2b plus ribavirin for initial treatment of chronic hepatitis C: a randomised trial. Lancet 2001;358:958–965.

6 Hadziyannis SJ, Sette H Jr, Morgan TR, Balan V, Diago M, Marcellin P, Ramadori G, Bodenheimer H Jr, Bernstein D, Rizzetto M, Zeuzem S, Pockros PJ, Lin A, Ackrill AM; PEGASYS International Study Group: Peginterferon-alpha2a and ribavirin combination therapy in chronic hepatitis C: a randomized study of treatment duration and ribavirin dose. Ann Intern Med 2004;140:346–355.

7 Enomoto N, Sakuma I, Asahina Y, Kurosaki M, Murakami T, Yamamoto C, Izumi N, Marumo F, Sato C, Asahina Y: Comparison of full-length sequences of interferon-sensitive and resistant hepatitis-C virus 1bd sensitivity to interferon is conferred by amino-acid substitutions in the NS5A region. J Clin Invest 1995;96:224–230.

8 Akuta N, Suzuki F, Sezaki H, Suzuki Y, Hosaka T, Someya T, Kobayashi M, Saitoh S, Watahiki S, Sato J, Matsuda M, Kobayashi M, Arase Y, Ikeda K, Kumada H: Association of amino acid substitution pattern in core protein of hepatitis C virus genotype 1b high viral load and non-virological response to interferon-ribavirin combination therapy. Intervirology 2005;48:372–380.

9 Shirakawa H, Matsumoto A, Joshita S, Komatsu M, Tanaka N, Umemura T, Ichijo T, Yoshizawa K, Kiyosawa K, Tanaka E; Nagano Interferon Treatment Research Group: Pretreatment prediction of virological response to peginterferon plus ribavirin therapy in chronic hepatitis C patients using viral and host factors. Hepatology 2008;48:1753–1760.

10 Conjeevaram HS, Kleiner DE, Everhart JE, Hoofnagle JH, Zacks S, Afdhal NH, Wahed AS, Virahep-C Study Group: Race, insulin resistance and hepatic steatosis in chronic hepatitis C. Hepatology 2007;45:80–87.
11 Ge D, Fellay J, Thompson AJ, Simon JS, Shianna KV, Urban TJ, Heinzen EL, Qiu P, Bertelsen AH, Muir AJ, Sulkowski M, McHutchison JG, Goldstein DB: Genetic variation in IL28B predicts hepatitis C treatment-induced viral clearance. Nature 2009;461:399–401.
12 Tanaka Y, Nishida N, Sugiyama M, Kurosaki M, Matsuura K, Sakamoto N, Nakagawa M, Korenaga M, Hino K, Hige S, Ito Y, Mita E, Tanaka E, Mochida S, Murawaki Y, Honda M, Sakai A, Hiasa Y, Nishiguchi S, Koike A, Sakaida I, Imamura M, Ito K, Yano K, Masaki N, Sugauchi F, Izumi N, Tokunaga K, Mizokami M: Genome-wide association of IL28B with response to pegylated interferon-alpha and ribavirin therapy for chronic hepatitis C. Nat Genet 2009;41:1105–1109.
13 Suppiah V, Moldovan M, Ahlenstiel G, Berg T, Weltman M, Abate ML, Bassendine M, Spengler U, Dore GJ, Powell E, Riordan S, Sheridan D, Smedile A, Fragomeli V, Müller T, Bahlo M, Stewart GJ, Booth DR, George J: IL28B is associated with response to chronic hepatitis C interferon-alpha and ribavirin therapy. Nat Genet 2009;41:1100–1104.
14 Enomoto N, Sakuma I, Asahina Y, Kurosaki M, Murakami T, Yamamoto C, Ogura Y, Izumi N, Marumo F, Sato C: Mutations in the nonstructural protein 5A gene and response to interferon in patients with chronic hepatitis C virus 1b infection. N Engl J Med 1996; 334:77–81.
15 Akuta N, Suzuki F, Kawamura Y, Yatsuji H, Sezaki H, Suzuki Y, Hosaka T, Kobayashi M, Kobayashi M, Arase Y, Ikeda K, Kumada H: Predictive factors of early and sustained responses to peginterferon plus ribavirin combination therapy in Japanese patients infected with hepatitis C virus genotype 1b: amino acid substitutions in the core region and low density lipoprotein cholesterol levels. J Hepatol 2007;46:403–410.
16 Okanoue T, Itoh Y, Hashimoto H, Yasui K, Minami M, Takehara T, Tanaka E, Onji M, Toyota J, Chayama K, Yoshioka K, Izumi N, Akuta N, Kumada H: Predictive values of amino acid sequences of the core and NS5A regions in antiviral therapy for hepatitis C: a Japanese multi-center study. J Gastroenterol 2009;44:952–963.
17 Hiramatsu N, Oze T, Yakushijin T, Inoue Y, Igura T, Mochizuki K, Imanaka K, Kaneko A, Oshita M, Hagiwara H, Mita E, Nagase T, Ito T, Inui Y, Hijioka T, Katayama K, Tamura S, Yoshihara H, Imai Y, Kato M, Yoshida Y, Tatsumi T, Ohkawa K, Kiso S, Kanto T, Kasahara A, Takehara T, Hayashi N: Ribavirin dose reduction raises relapse rate dose-dependently in genotype 1 patients with hepatitis C responding to pegylated interferon alpha-2b plus ribavirin. J Viral Hepat 2009; 16:586–594.
18 Oze T, Hiramatsu N, Yakushijin T, Kurokawa M, Igura T, Mochizuki K, Imanaka K, Yamada A, Oshita M, Hagiwara H, Mita E, Ito T, Inui Y, Hijioka T, Tamura S, Yoshihara H, Hayashi E, Inoue A, Imai Y, Kato M, Yoshida Y, Tatsumi T, Ohkawa K, Kiso S, Kanto T, Kasahara A, Takehara T, Hayashi N: Pegylated interferon alpha-2b (Peg-IFN alpha-2b) affects early virologic response dose-dependently in patients with chronic hepatitis C genotype 1 during treatment with Peg-IFN alpha-2b plus ribavirin. J Viral Hepat 2009; 16:578–585.
19 Nakagawa M, Sakamoto N, Ueyama M, Mogushi K, Nagaie S, Itsui Y, Azuma S, Kakinuma S, Tanaka H, Enomoto N, Watanabe M: Mutations in the interferon sensitivity determining region and virological response to combination therapy with pegylated interferon alpha 2b plus ribavirin in patients with chronic hepatitis C-1b infection. J Gastroenterol 2010;45:656–665.
20 Nakano I, Fukuda Y, Katano Y, Nakano S, Kumada T, Hayakawa T: Why is the interferon sensitivity-determining region (ISDR) system useful in Japan? J Hepatol 1999;30: 1014–1022.
21 Hayashi K, Katano Y, Ishigami M, Itoh A, Hirooka Y, Nakano I, Urano F, Yoshioka K, Toyoda H, Kumada T, Goto H: Mutations in the core and NS5A region of hepatitis C virus genotype 1b and correlation with response to pegylated-interferon-alpha 2b and ribavirin combination therapy. J Viral Hepatol 2011; 18:280–286.
22 Zeuzem S, Lee JH, Roth WK: Mutations in the nonstructural 5A gene of European hepatitis C virus isolates and response to interferon alfa. Hepatology 1997;25:740–744.
23 Squadrito G, Raffa G, Restuccia T, Pollicino T, Brancatelli S, Raimondo G: Is investigation of hepatitis C virus NS5A gene heterogeneity a tool for predicting long-lasting response to interferon therapy in patients with HCV-1b chronic hepatitis? J Viral Hepatol 2002;9:360–369.

Jpn. J. Appl. Physics, No.7, 2012. (to be published)

Mechanical Model Analysis for Quantitative Evaluation of Liver Fibrosis based on Ultrasound Tissue Elasticity Imaging

Tsuyoshi Shiina, Tomonori Maki, Makoto Yamakawa[1], Tsuyoshi Mitake[2], Masatoshi Kudo[3], Kenji Fujimoto[4]

Human Health Sciences, Graduate School of Medicine, Kyoto University.
Kawahara-cho, Shogoin, Sakyo-ku, , Kyoto 606-8507, Japan.
[1]Advanced Biomedical Engineering Research Unit, Kyoto University.
Yoshida-honmachi, Sakyo-ku, Kyoto 606-8501, Japan.
[2]HitachiAlokaMedicalLtd.Shin-toyoni, Kashiwa, Chiba 227-0804, Japan
[3]Department of Gastroenterology and Hepatology, Kinki University School of Medicine.
Ohno-higashi, Osaka-sayama, Osaka, 589-8511 Japan.
[4]Department of Internal Medicine, National Hospital Organization, Minami-Wakayama Medical Center. Tanabe, Wakayama, Japan.

Abstract—Precise evaluation of the stage of chronic hepatitis C with respect to fibrosis has become an important issue to prevent the occurrence of cirrhosis and to initiate appropriate therapeutic intervention such as viral eradication using interferon. Ultrasound tissue elasticity imaging, i.e., elastography can visualize tissue fibrosis progression and simulated the process that hepatic fibrosis affects elasticity images and compared clinical data analysis. As a result, it was confirmed that even in diffuse diseases like chronic hepatitis, pattern of elasticity image is related with fibrous structure change caused by hepatic disease and can be used to derive features for quantitative evaluation of fibrosis stage.

1. Introduction

Chronic liver damage attributable to Hepatitis C virus (HCV) infection results in hepatic fibrosis, which progresses towards cirrhosis, leading to hepatocellular carcinoma and more than 40,000 people every year die of cirrhosis and hepatic carcinoma in Japan.[1)] Thus, a precise evaluation of the stage of chronic hepatitis C with respect to fibrosis is an important issue to prevent the occurrence of cirrhosis and to initiate appropriate therapeutic intervention such as viral eradication using interferon[2)].

At present, liver biopsy is still the gold standard for the assessment of liver fibrosis. However, it is an invasive method associated with patient discomfort and, in rare cases, with serious complications.[3,4)] In addition, the accuracy of liver biopsy is limited because of significant intra- and interobserver variability and sampling errors.[5–7)] Therefore, research has been focused on the evaluation of noninvasive methods for the assessment of liver fibrosis.

Image diagnosis using B-mode image have been conventionally applied for diagnosis of liver disease. However, it is not easy to diagnosis its early stage by conventional B-mode image because we have to read hardness/softness, and its clinical usefulness has been studied to detect and evaluate tumour. We recently reported that texture of elasticity image changes as fibrosis progresses. In order to evaluate fibrosis progression quantitatively based on ultrasound tissue elasticity imaging, we introduced a mechanical model of subtle change of speckle pattern which is not sensitive to the stage of fibrosis.

To overcome this problem, there has been considerable research on quantitative assessment of liver fibrosis based on ultrasonography such as echo signal processing and texture analysis method.[8,9)] Yamaguchi and Hachiya[10-12)] recently proposed the method to evaluate the stage of fibrosis using the deviation of echo amplitude distribution form Rayleigh distribution of a normal liver.

From a viewpoint of directly measuring the stiffness of liver tissue, we investigated the application of tissue elasticity imaging to evaluation of fibrosis stage. Ultrasonic tissue elasticity imaging can provide us novel diagnostic information based on tissue hardness.[13-15)] Although the first practical system is developed by Shiina et al. for tumor diagnosis, Fujimoto et al. recently reported that the pattern of elasticity image becomes patchy as fibrosis progresses in the case of diffuse diseases like chronic hepatitis.[16)] We also proposed the Liver fibrosis (LF) Index which was derived from elasticity image, and showed that there was a good correlation between the LF index and the degree of liver fibrosis.[16-18)]

In order to evaluate fibrosis progression quantitatively based on the strain image, it is important to clarify how fibrosis progression affects the dynamic properties of liver tissues and are consequently shown in the elasticity image. In this paper, we introduced a mechanical model of fibrosis progression and simulated the process that hepatic fibrosis affects elasticity images and compared clinical data analysis. As a result, it was

confirmed that even in diffuse diseases like chronic hepatitis, pattern of elasticity image is related with fibrous structure caused by hepatic disease and can be used to derive features for quantitative evaluation of fibrosis stage.

2. Methos

2.1 Evaluation of liver fibrosis by ultrasound tissue elasticity imaging

It is well known that chronic liver disease causes hepatic fibrosis, which is characterized by an unusual accumulation of extracellular matrix materials produced by fibroblast-like cells including stellate cells in the hepatic parenchyma. Diagnosing chronic liver disease in early stage is necessary to treat liver disease because hepatic cirrhosis often causes other diseases such as liver cancer. In terms of stage of chronic hepatitis, the New Inuyama scoring system was used, which was proposed by the Japanese Liver Study Group in 1994.[19] The New Inuyama scoring system classifies the chronic hepatitis into five fibrosis stage (F0-F4) based on the extent of spreading fibrosis and four grade (A0-A3) based on degree of inflammation and necrosis using liver biopsy samples as shown in Table 1.

Recently, the ultrasound systems for measurement and imaging of tissue elasticity have been developed as non-invasive methods to evaluate the degree of liver fibrosis, providing alternatives to liver biopsy. FibroScan® (Transient elastography) detects the propagation speed of a shear wave transmitted from a probe through the liver and calculates the shear modulus of the liver to evaluate the degree of liver fibrosis.[20] Although FibroScan® is simple and easy to use and displays the results on a monitor immediately, it has also many limitations. It cannot be used in patients with narrow intercostal spaces, hepatic atrophy and ascites since shear waves will not propagate through flues.[21,22] In addition, it is difficult to locally evaluate the degree of fibrosis since the result is based on 1-dimensional information (1-line) only.

Ultrasound tissue elasticity imaging is developed for the visual assessment of tissue elasticity especially for cancer diagnosis. The first practical system was developed by us and employs the algorithm referred to as the Combined Autocorrelation Method proposed by Shiina *et al.* [23,24] The method can rapidly calculate a 2-dimensional distribution of the tissue deformation, i.e., strain induced by external freehand compression with the probe or by internal heartbeats. In hard tissue, the amount of strain is low, whereas in soft tissue, the amount of strain is higher because soft tissue can be compressed more than hard tissue. However, the strain is relative hardness since it changes with compression level. For stable display of the strain distribution free of compression variation, the strain is normalized by the mean value within ROI, ε_0 , and displayed with translucent color superimposed on the B-mode image (soft: red /mean: green/ hard: blue), as illustrated in Fig.1. This method is commercialized in 2003, and referred to as the Real-Time Tissue Elastography® (RTE).[15] At present, several companies have released the tissue elasticity imaging system and different methods for imaging are adopted.

This technology has already been proved to be diagnostically valuable in detecting tumour of the breast, prostate and other organs.[25] We found that texture of elasticity image (strain) of chronic hepatitis becomes patchy pattern as liver fibrosis progress and could be categorized into the four stages as shown in Fig. 2.[16,17] The strain induced by heartbeats (diastole) is used to perform RTE. Hepatic fibrosis progresses towards cirrhosis, which causes the fine liver lobule structure to change to a coarse nodular structure stage by stage. The size of the nodules and the volume of the fibers changes with the progression of disease. Considering this process of fibrosis, it is expected that fibrosis cause the inhomogeneous distribution of tissue hardness, which produces non-uniform texture pattern of strain images.

However, it is limited to quantitatively evaluate the texture pattern by visual judgement. To increase objectivity, we extract nine image features as shown in Fig.3. First of all, the region of interest (ROI) was fixed to a rectangle with about 30 mm x 20 mm. Pixel data in the colored strain image was transformed into a histogram. Finally, we performed multiple regression analysis to derive the index of liver fibrosis (LF index) as to major four features as follows,

$$\text{LF index} = a_1\,\text{MEAN} + a_2\,\text{SD} + a_3\,\%\text{AREA} + a_4\,\text{COMP} \quad (1)$$

Major four features were extracted as follows; MEAN is mean of relative (normalized by ε_0) strain value, SD is Standard deviation of relative strain value, which are calculated from strain histogram. The strain image is transformed into binary image, then blue or low strain which indicates hard area is detected. %AREA indicates the percentage of low strain area (white region in the Fig. 3(c)) in the ROI. COMP is complexity of the shape of an extracted low strain area and is defined by Eq.(1),

$$\text{COMP} = \frac{L^2}{S} \quad (2)$$

where, L is boundary length of low strain area, S is area of low strain region.

So far, we performed RTE on 310 cases including 295 patients with chronic hepatitis C and 15 healthy volunteers. As a result, the coefficient of LF index , a_1 = - 0.00897, a_2= - 0.00502, a_3= 0.0232, a_4 = 0.0253 were obtained. It was confirmed that The LF Index highly correlated with the fibrous stage as shown in Fig.2.[16]

2.2 Mechanical model analysis of liver fibrosis

In order to clarify how fibrosis progression affects the elasticity image of chronic hepatitis, we analysed the relation by simulating the process with mechanical model of hepatic fibrosis. At first, the structural change of liver tissue by fibrous progression is simulated as shown in Fig.

4. Next, the change of tissue stiffness and deformation by compression are simulated. Finally, the imaging process and feature extraction by RTE are reconstructed to compare the results with clinical cases.

2.2.1 Modeling of tissue structure change

The human liver is composed of many hexagonal structures termed liver lobules and containing a central vein. Fibrosis progression is accompanied by changes of tissue structure. When fibrosis grows, the lobules are destroyed and replaced by regenerative nodules.

In terms of the modeling of the liver tissue structure change by fibrous progression, Yamaguchi *at al.* have proceeded many researches and proposed a model using the potential distribution.[11] We referred the potential distribution model as a part to simulate tissue structure change. In this model, scatterers are distributed densely on the local minimum region of the monomodal potential function as expressed by Eq. (3) and the position of its peak corresponds to central points of liver nodule.

$$p(r) = p_{\max} \sin\left(\frac{\pi}{2} k^r\right) \tag{3}$$

where, r is distance from the central point, $p_{\max}$ is the maximal value and k is the form parameter that determines the distribution spread. The parameter $p_{\max}$ of all the potentials is defined as the value of 0.8 to 1.2 randomly as an initial condition and k is set to 0.02 + 0.002 $p_{\max}$ as experimentally estimated values as discussed in ref. 11.

In order to simulate the process that liver tissue changes from lobules to nodule, the randomly selected central point, r_m conjugates with its nearest central point, r_n, generating new central point, r_m' and new potential, $p_{\max}(r_m')$ as follows,

$$r_m' = (\alpha r_n + \beta r_m)/(\alpha + \beta) \tag{4}$$
$$p_{\max}(r_m') = \alpha + \beta \tag{5}$$

where, $\alpha = p_{\max}(r_m)$, $\beta = p_{\max}(r_n)$.

As a result, fiber tissues generated by conjugation are represented as the minimum region of the potential distribution.

2.2.2 Modeling of tissue elasticity

To simulate tissue deformation, finite element method (FEM) is applied to the tissue model. For FEM analysis, the region of interest (30mm x 30mm) is divided in a recticular pattern and 500 x 500 elements, consequently, the element size was 0.06 mm x 0.06 mm which can attain the adequate spatial resolution for stain image. First of all, values of Young's modulus are assigned to each grid point of the structural model in 2.2.1. as follows,

$$E_p(x,y) = \alpha(p_{\max} - \bar{p}_{\max,normal})^n + E_{normal}$$
(for parenchyma) (6)
$$E_f(x,y) = \beta(p_{neighbor\max} - \bar{p}_{\max,normal})^n + E_{normal}$$
(for fibroic region) (7)

where, parenchyma represents the region of lobule and nodule except for fibroic region. $\bar{p}_{\max,normal}$ is the average of the maximal value of each potential for a normal liver model, and E_{normal} is the average of Young's modulus on parenchyma of a normal liver model. $p_{neighbor\max}$ is defined as,

$$p_{neighbor\max} = p_{\max,k}$$
$$\text{for } \{k \mid \max\left(\frac{p_{\max,i}}{d_i^2}\right),\ i = 1,2\cdots M\}$$

where, $p_{\max,i}$ (i=1,2,...M) are maximal values of potential neighbor to the grid point located within fibrous region and d_i is the distance between the grid point and each central point of potential.

Here, E_{normal} is set to 4 [kPa] using the experimentally measured values by FibroScan® as shown in Table.2.[26-28] Parameter α, β indicate weight of the potential contributes to Young's modulus. Parameter n regulates the rate of stiffness increase, that is, in case of n=1, E increases in proportion to conjugated potential and in case of n=2, E increases nonlinearly.

2.2.3 Modeling of tissue deformation

The Young's modulus distribution model is compressed from upper with pressure which causes a slight stain as much as clinical examination (about 1%) and Poisson ratio of tissue model is set to 0.49. The tissue deformation, that is, movement of each node of element is simulated by FEM assuming the two-dimensional stress state. Displacement of nodes along axial direction is calculated by comparison of two frame data before and after compression. Then, the strain is calculated by differential processing of the displacement. The obtained strain distribution is color-coded and displayed as same as RTE.

2.2.4 Feature extraction

For the purpose of evaluating how the tissue stiffness change caused by fibrosis progression is related to the strain distribution, the strain image is directly reconstructed from displacement by FEM analysis in 2.2.3. It is required to simulate the signal processing of ultrasound equipment (RTE) since in practice, the strain distribution must be estimated from echo signals.

The number of scatterers distributed within 30mm x 30mm was set to 4500, that is, the density is 5 points/mm^2 and the scattering coefficient is set based on tissue structural model. The position of each scatterers after compression is obtained from the position of nodes as a result of FEM analysis. RF echo signals are generated by using the transmitted pulse with Gaussian envelope, the center frequency of 5MHz and duration of 0.4mm. The beam width is set to 0.8 mm.

Then, the strain distribution is calculated by the combined autocorrelation method and the normalized strain is color-coded as RTE.

Finally, major four features were extracted from the strain image and LF index was calculated to compare the results with clinical cases.

3. Results and discussion

Figure 5 illustrates the fibrous structure of normal and chronic hepatitis obtained based on modeling of tissue structure change. Two-dimensional model was applied and 2538 central points were distributed within area (40mmx40mm), in other words, liver lobules were located at 0.8mm mean interval. Figure 5 (a) presents the normal liver, and (b) - (e) depict the liver tissue structure when fibrosis progresses. The number of iteration does not indicate the physical characteristic of the liver directly, but is selected to only determine the size of nodules. Here, the conjugating process was repeated until the number of central points reduced to 1/2 (F1), 1/4 (F2), 1/8 (F3) , 1/16 (F4) of the initial central points simply assuming that average number of conjugation is 1,2,3,4 times for each stage. We can observe that the sizes of the nodules and the widths of the fibers increase with the progression of liver fibrosis and inhomogeneous structures are also evident in serious cases.

Figure 6 illustrates the Young's modulus distribution assigned to the models in Fig.5. The range of Young's modulus for each image is indicated at the bottom in Fig.6. Parameters in Eqs.(6),(7) were set to n=1 and $\alpha = \beta$ = 1.3, so that the mean values of Young's modulus assigned for each stage was close to values measured by FibroScan®as shown in Table 3.

As fibrosis progresses, the maximum potential $p_{\max}$ becomes higher, so assigned values of Young's modulus $E(x,y)$ increase accordingly due to eqs. (5), (6). As a result, it can be seen that the region around large size of nodule has the large values of Young's modulus, namely, becomes hard in Fig. 6.

The tissue model of Fig.6 was compressed on the top by 50 Pa (1.25% of E_{normal} =4kPa) in the axial direction. Then, strain images ware obtained as shown in Fig.7. The top are strain images reconstructed directly from the displacement obtained by FEM analysis. The bottom shows images estimated from generated echo signals by simulating RTE. Compared with strain image by FEM, display area of strain image by RTE is smaller (28.5 mm x 21.6 mm) since marginal parts are used for estimation. It can be seen that as fibrosis progresses, the blue area increases, indicating that the area has become stiffer than the area around it. In addition, the strain distribution becomes more and more complex.

Figure 8 represents the mean strain within the analyzing area for each stage. We can see that the mean strain decreases as the stage progresses. It should be noted that strain images by FEM reflect the pattern of Young's modulus distribution in Fig.6. In addition, there is naturally a good correlation between both strain images although strain images by RTE are blurred than those by FEM since the former are estimated from echo signals.

Finally, four features extracted from strain image (RTE) and LF index derived using Eq.(1) as a function of fibrosis stage are shown in Fig. 9. For the simulation in Fig.9 (a)-(e), a parameter n in Eq.(6) was set to 1 as well as Fig.6 and Fig.7. It can be observed that MEAN decrease, while SD, %AREA increase as fibrosis progresses. COMP seems to become large for serious case. As shown in Fig.9 (e), LF index derived these features also tends to increase. The relation of LF index and fibrosis stage obtained by clinical data analysis for 310 cases is shown in Fig.9 (f). Although the result of simulation analysis is for a single case, LF index obtained using mechanical model of fibrosis progression coincides with result of the clinical data analysis.

These results indicate that even in diffuse diseases like chronic hepatitis, pattern of strain image is related with fibrous structure change caused by hepatic disease and can be used to derive features for quantitative evaluation of fibrosis stage.

On the other hand, there remains several problems to be solved for development of clinically useful method. For example, parameters of models described in 2.2.1 and 2.2.2 are defined to only determine the size of the nodules or rate of stiffness increase. Therefore, they do not directly indicate the physical characteristic of the liver. Especially, the number of iteration is important parameter, there is no a priori information at present. In terms of a parameter n, representing the rate of stiffness increase, if parameters are set to n = 2, $\alpha=\beta=0.1$, the staging is accelerated as shown in Fig. 10. To tune or optimize these parameters, it is indispensable to continue the simulation for several conditions and compare the results with a large number of clinical data.

As mentioned in 2.1, chronic hepatitis is scored by fibrosis staging and grading. Our clinical research validates that LF index by RTE stably reflects the fibrosis stage without influenced by variables of inflammatory state or blood pressure. On the other hand, it is reported that the values measured by FibroScan® are influenced by variables such as hepatic steatosis, and flares of transaminases.[21,22] This indicates that shear wave velocity is also changed by other factors than fibrosis stage. In terms of shear wave velocity measurement, some methods using acoustic radiation force for shear wave generation within body are recently developed such as Acoustic Radiation Force Impulse (ARFI) imaging[29] and Shear Wave Elastography (SWE).[30] These methods also can be used as a noninvasive method of assessing tissue stiffness and it is expected to utilize different diagnosis information by using both methods, that is, strain image and shear wave image.

4. Conclusion

This study proposed a mechanical model of fibrosis progression. From the strain distribution, we could see that the area of low strain increases, and the strain distribution becomes more and more complex as fibrosis progresses. Extracted features of strain and derived Liver Fibrosis Index showed definite tendency as a fibrosis progression and coincided with result of clinical data

analysis.These indicate that even in diffuse diseases like chronic hepatitis, pattern of strain image is related with fibrous structure change caused by hepatic disease and can be used to derive features for quantitative evaluation of fibrosis stage.

As above mentioned, to optimize the parameters used for simulation analysis, it is indispensable to continue the simulation for several conditions and compare the results with a large number of clinical data. For example, although the number of iteration for conjugating process does not directly indicate the physical characteristic of the liver, the %AREA may be useful reference to relate the number of iteration to fibrosis stages. Figure 11 shows the %AREA obtained by clinical data analysis, which increases as a function of fibrosis stage and is similar to Fig.9 (c).

In addition, for future work, there remain some problems to be investigated. To extract reliable diagnosis information from strain image, the stable data acquisition system that is robust to noise and artifact must be developed. In order to improve the precision of simulation, we must investigate the way to obtain the precise values of Young's modulus for each component, such as parenchyma and fibrous portion, for example, by microscopic measurement of tissues for each stage of hepatitis. Finally, in terms of extraction of image features, it is one of most important theme of this research to extract more appropriate features to be useful for precise diagnosis of chronic hepatitis.

References

1) A.Ohshima : Proc. of 123rd Symposium of the Japanese Association of Medical Sciences, 2003, p.13 [in Japanese].
2) National Institutes of Health Consensus Development Conference Statement. Management of hepatitis C: Hepatology, **36** [5suppl 1] (2002) S3.
3) A.A. Bravo, S.G. Sheth, S.Chopra: New Engl. J. Med. **344** (2001) 495.
4) I. Sporea , A. Popescu, R. Sirli. : World J Gastroenterol., **14** (2008) 396
5) P. Bedossa, D. Dargere, V. Paradise: Hepatology, **38**(2003) 1449.
6) M. Ziol, A. Handra-Luca, A. Kettaneh, C. Christidis, F. Mal, F. Kazemi, V. de Ledinghen V. P. Marcelin, D. Dhumeaux, J.C, Trinchet, M Beaugran: Hepatology 41(2005) 48.
7) U. Arena, F. Vizzutti, G. Corti, S. Ambu, C. Stasi, S. Bresci, S. Moscarella, V. Boddi, A. Petrarca, G. Laffi, F. Marra, M. Pinzani : Hepatology. 47 (2008) 380.
8) Y. Fujii, N. Taniguchi, K. Itho: Medical Imaging Technology **21**(2003) 117.
9) T. Nishimura, H. Watanabe, M. Ito, Y. Matsuoka, K. Yano, M. Daikoku, H. Yaysuhasshi, K. Dohmen, H. Ishibashi: British J. of Radiology **78** (2005) 189.
10) T. Yamaguchi, H. Hachiya, K. Kato, H. Fukuda, and M. Ebara: Jpn. J. Appl. Phys. **39**(2000) 3266.
11) T. Yamaguchi, K. Nakamura, H. Hachiya: Jpn. J. Appl. Phys. **42** (2003) 3292.
12) Y. Igarashi, H. Ezuka, T. Yamaguchi, H. Hachiya: Jpn. J. Appl. Phys. **49** (2010) 07HF06.
13) T. Shiina, N. Nitta, E. Ueno, J.C.Bamber : J. Med. Ultrasonics **29** (2002) 119.
14) M. Yamakawa, N. Nitta, T. Shiina, M. Matsumura, S. Tamano, T. Mitake, E. Ueno: Jpn. J. App. Phys. **42** (2003) 3265.
15) A. Itoh, E. Ueno, E. Tohno, H. Kamma, H. Takahashi, T. Shiina, M. Yamakawa, T. Matsumura: Radiology **231** (2006) 341.
16) K. Fujimoto, M. Kato, A. Tonomura, N. Yada, C. Tatsumi, M. Oshita, S. Wada, K. Ueshima, T. Ishida, T. Furuta, M. Yamasaki, M. Tsujimoto, M. Motoki, T. Mitake, S. Kim, K. Yamamoto, T. Shiina, M. Kudo, N. Hayashi: Kanzo **51**(2010) 539 [in Japanese].
17) A. Tonomura, M. Motoki, T. Mitake, K. Fujimoto, M. Kato, C. Tatsumim, N. Yada, K. Ueshima, M. Kudo, T. Shiina: Proc. 22nd Kanto-section meeting of JSUM (2010) 36 [in Japanese].
18) C. Tatumi, M. Kudo, K. Ueshima, S. Kitai, E. Ishikawa, N. Yada, S. Hagiwara, T. Inoue, Y. Minami, H. Chung, K. Maekawa, K. Fujimoto, M. Kato, A. Tonomura, T. Mitake, T. Shiina: Intervirology **53** (2010) 76.
19) F. Ichida, T. Tsuji, M. Omata, T. Ichida, K. Inoue, T. Kaminuma, G. Yamada, K. Hino, O. Yokosuka, H. Suzuki: Int. Hepatology Communications **36** (1996) 112.
20) L. Sandrin, B. Fourquet, J.M. Hasquenoph, S. Yon, C. Fournier, F. Mal, C. Christidis, M. Ziol, B. Poulet, F. Kazemi, M. Beaugrand, R. Palau: Ultrasound Med Biol. **29**(2003) 1705.
21) M. Friedrich-Rust, M. F. Ong, S. Martens, C. Sarrazin, J. Bojunga, S. Zeuzem, E. Herrmann: Gastroenterology **134**(2008) 960.
22) U. Arena, F. Vizzutti, G. Corti, S. Ambu, C. Stasi, S. Bresci, S. Moscarella, V. Boddi, A. Petrarca, G. Laffi, F . Marra, M. Ponzani: Hepatology, **47** (2008) 380.
23) T. Shiina, M. M. Doyley, J. C. Bamber: Proc. of 1996 IEEE Ultrasonics Symposium (1997) 1331.
24) M. Yamakawa, T. Shiina: Jpn. J. Appl. Phys. **40** (2001) 3872.
25) E.Tohno, E. Ueno: Breast Cancer **15** (2008) 200.
26) National Center for Global Health and Medicine, Disease Control and Prevention Center, Home Page (2008) (http://www.ncgm.go.jp/center/formedsp_cir.html) [in Japanese].
27) T. Yasuda, T. Takeda, Y. Nakayama, K. Uehata, H. Sakaguchi, M. Seki, A. Sawada, M. Yamashita, K.Abo, S. Takeda, H. Asai: presented at the 151st Osaka Abdomen Ultrasound, 2005. [in Japanese]
28) M. Ziol, A. Handra-Luca, A. Kettaneh, C. Christidis, F. Mal F, F. Kazemi, V. de Lédinghen, P. Marcellin, D. Dhumeaux, J. C. Trinchet, M. Beaugrand: Hepatology 41(2005) 48.
29) M. L. Palmeri, M. H. Wang, J. J. Dahl, K. D. Frinkley, K. R. Nightingale: Ultrasound Med Biol. **34** (2008) 546.
30) J. Bercoff, M. Tanter, M. Fink: IEEE Trans Ultrason Ferroelectr Freq Control **51** (2004) 396.

List of Figures and Tables

Table 1. The New Inuyama scoring system

Staging (fibrosis)		Grading (necrosis and inflammation)	
F0	no fibrosis,	**A0**	no
F1	fibrous portal expansion	**A1**	mild
F2	bridging fibrosis	**A2**	moderate
F3	bridging fibrosis with lobular degeneration	**A3**	severe
F4	cirrhosis		

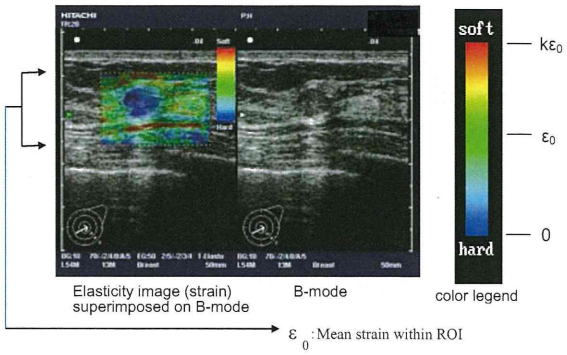

(Color) Fig.1 Display method of elasticity image

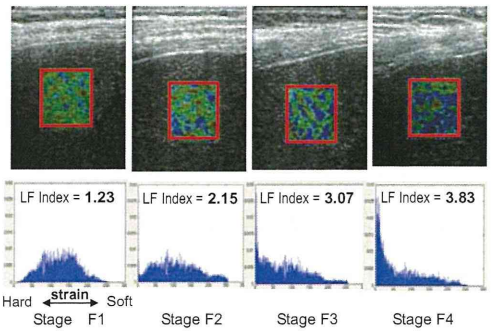

(Color) Fig. 2 Elasticity images (strain) superimposed on B-mode (top) and histogram of the strain distribution within ROI (bottom) for each fibrosis stage of chronic hepatitis

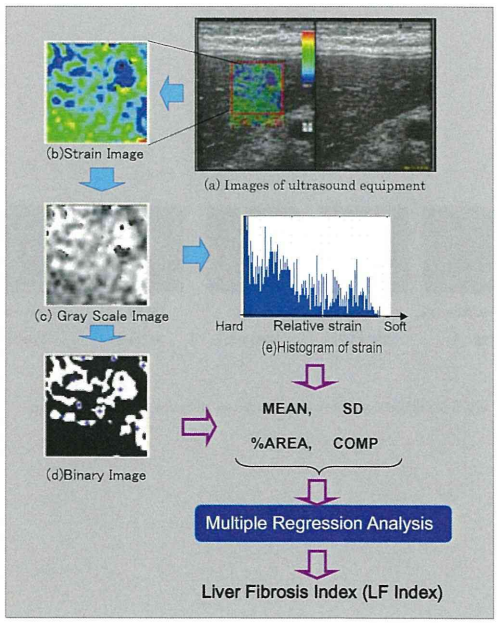

Nine features
1. MEAN : Mean of relative strain value
2. STD : Standard deviation of relative strain value
3. %AREA : Ratio of blue area in analysis region
4. COMP : Complexity of blue area
5. SKEW : Asymmetry of the histogram
6. KURT : Peakedness of the histogram
7. ENT : Textual complexity
8. IDM : Textual local homogeneity (Inverse Difference Moment)
9. ASM :Textual homogeneity (Angular Second Moment)

(Color) Fig. 3 Extraction of image features from strain image and Liver Fibrosis Index (LF Index) for quantitative evaluation of fibrous progression.

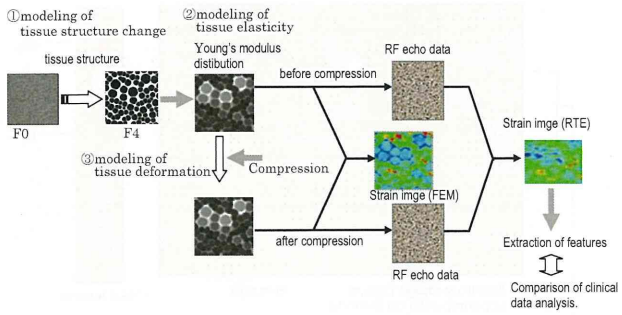

(Color) Fig.4 Analysis of liver fibrosis progression and its influence on strain imaging using mechanical model.

Table 2. Elastic modulus of liver tissues measured at each fibrous stage

Fibrous stage	F0	F1	F2	F3	F4
Young's modulus Measured by FibroScan® [kPa]	< 5	7	13	18	22
	4.2	6.9	8.9	14.8	26.5
(top[26], middle[27] bottom[28])	5.5		6.4	10.0	30.0

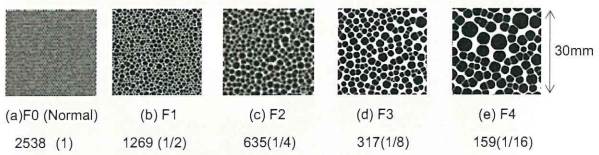

Fig. 5 Simulated tissue structure change caused by the fibrous progression

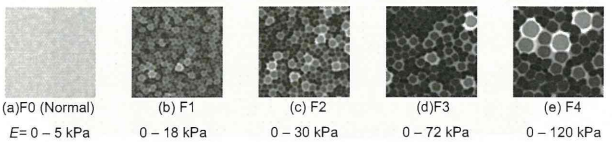

Fig. 6 Young's modulus distribution assigned to tissue structure model

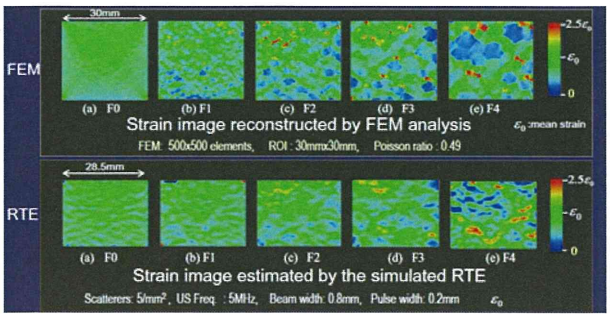

(Color) Fig. 7 Strain images obtained by FEM analysis and simulated RTE

Table 3. Comparison of elastic modulus between model and measured values

Fibrous stage	F0	F1	F2	F3	F4
Mean values of Young's modulus set to the model [kPa]	4.0	6.2	10.0	17.1	35.7
Young's modulus Measured by FibroScan® [kPa] (averaged values of Ref. 26-28)	4.9	6.5	9.4	14.3	26.2

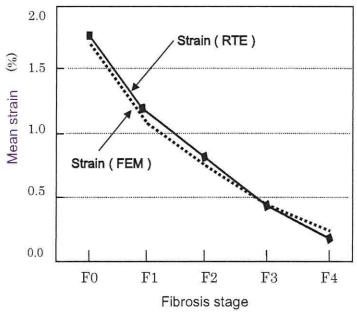

Fig.8 Change of mean values of strain

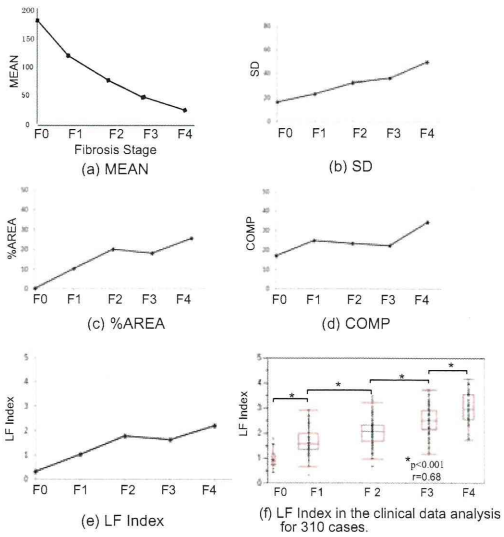

Fig.9 Features of strain image and LF Index as a function of fibrosis stage in the case of n=1, $\alpha = \beta = 1.3$ (parameter in Eq. (6),(7)).

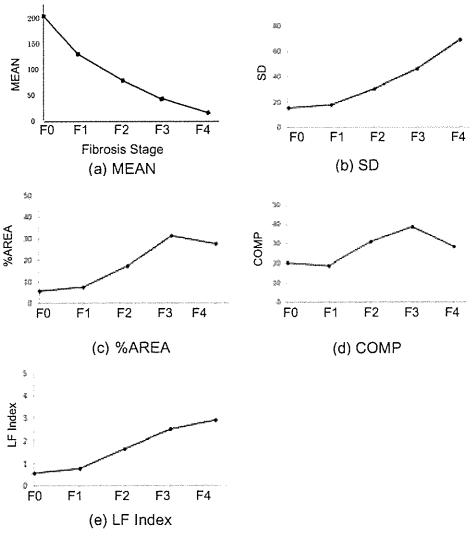

Fig.10 Features of strain image and LF Index as a function of fibrosis stage in the case of n=2, $\alpha = \beta = 0.1$ (parameter in Eq. (6),(7)).

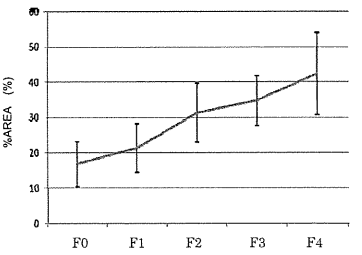

Fig.11 Change of %AREA as a function of fibrosis stage (clinical data analysis)

PROCEEDINGS

of the

Tenth International Tissue Elasticity Conference™

Arlington, Texas, USA
October 12–15, 2011

Table of Contents

066 **MECHANICAL MODEL ANALYSIS FOR QUANTITATIVE EVALUATION OF LIVER FIBROSIS BASED ON REAL-TIME TISSUE ELASTOGRAPHY.**

Tsuyoshi Shiina[1], Makoto Yamakawa[2], Masashi Kudo[3], Akiko Tonomura[4], Tsuyoshi Mitake[4].*
[1]Graduate School of Medicine, [2]Advanced Biomedical Engineering Research Unit, Kyoto University, Kyoto, JAPAN; [3]Gastroenterology and Hepatology Department, Kinki University School of Medicine, Osaka-Sayama, JAPAN; [4]Hitachi Aloka Medical, Ltd., Chiba, JAPAN.

Background: Chronic liver damage attributable to hepatitis C virus (HCV) infection results in hepatic fibrosis, which progresses towards cirrhosis, leading to hepatic carcinoma. Thus, precise evaluation of the stage of chronic hepatitis C with respect to fibrosis has become an important issue in preventing the occurrence of cirrhosis and in initiating the appropriate therapeutic intervention. Tissue elasticity imaging is expected to provide a noninvasive approach for staging disease progression. We have developed commercial-based equipment for tissue elasticity imaging (Real-time Tissue Elastography, Hitachi) for detecting tumors in the breast, prostate, etc. Considering the process of fibrosis, it is expected that fibrosis causes the inhomogeneous distribution of tissue hardness, which produces the non-uniform texture pattern in strain images. We recently reported that the texture of an elasticity image is based on strain changes as cirrhosis progresses [1,2].

Aims: The goal of this study is to clarify how fibrosis progression is reflected in the elasticity image by using mechanical models of hepatic fibrosis and to evaluate fibrosis progression quantitatively based on tissue elasticity imaging.

Methods: Progression of hepatic fibrosis causes the fine liver lobule structure to change to a coarse nodular structure stage by stage [3]. The fibrous progression model was constituted to simulate the process of lobule conjugation to nodules. Young's modulus at the lobule and nodule is set to values determined by considering the experimentally measured data. Next, the tissue deformation model was constituted to calculate the tissue deformation caused by compression using the finite-element method (FEM). Finally, the strain was calculated by comparing two frames of data acquired before and after compression. The obtained strain distribution is color-coded and displayed as elastography. Simulation was performed to verify the feasibility of the proposed model. For the model of normal liver, 2538 central points of liver lobules were distributed within a 40x40mm area; the distance between lobules was about 1mm. Conjugation is repeated until a specified limit of nodule size.

Results: Figure1a depicts the fibrous structure for stage 1 and stage 3 chronic hepatitis obtained based on the fibrous progression model. Figure 1b presents the Young's modulus distribution assigned based on the tissue-deformation model. The strain distribution obtained by FEM analysis for each fibrous stage is shown in Figure 1c. Results of this simulation validate the assumption that fibrosis causes a non-uniform texture pattern in strain images. The mean values of strain within ROI decreases as fibrosis progresses as shown in Figure 2.

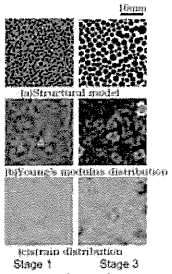

Figure 1: Examples of images obtained by using models of fibrous progression and tissue deformation.

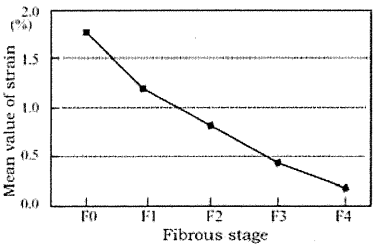

Figure 2: Relation between the mean values of strain and fibrous stage derived from simulation analysis.

Conclusions: As a result of the simulation of fibrosis progression using mechanical model of hepatic tissue, we confirmed that the strain image pattern is related to the change of fibrous structure and elastic modulus distribution caused by hepatic disease. For further investigation, it is necessary to quantitatively examine the relation and develop CAD system for chronic hepatitis based on ultrasound tissue elasticity imaging.

Acknowledgements: This work was supported by Grant-in-Aid for Science Research [22103507], Mext, Japan.

References:

[1] M. Yamazaki, H. Takizawa, T. Shiina: Computer-Aided Diagnosis of Diffuse Disease Based on Ultrasound Elasticity Images. Proc. of 2008 IEEE Int. Ultrasonics Symp., pp. 2033-2035, 2008.
[2] Chie Tatumi, Masatoshi Kudo, et al.: Noninvasive Evaluation of Hepatic Fibrosis for Type C Chronic Hepatitis. Intervirology, Vol. 53, pp.76-81, 2010.
[3] T. Yamaguchi, K. Hirai, et al.: Evaluation of Ultrasonic Fiber Structure Extraction Technique using Autopsy Specimens of Liver. Jap. J. of App. Phys., Vol. 44, pp. 4615-4621, 2005.

* *indicates Presenter*

2Pa5-4

Proceedings of Symposium on Ultrasonic Electronics, Vol. 32 (2011) pp. 141-142
8-10 November, 2011

Analysis of Elasticity Image of Chronic Hepatitis Based on Dynamic Model of Fibrosis Progression

肝線維化の力学的モデルに基づく肝エラストグラフィの解析

Tomonori Maki[1‡],Tsuyoshi Shiina[1],Makoto Yamakawa[2], Tsuyoshi Mitake3, Masatoshi Kudo[4] , Kenji Fujimoto[5] ([1]Grad. Sch. of Med., Kyoto Univ., [2]Advanced Biomed. Eng. Res. Unit, Kyoto Univ., [3]Hitachi Aloka Medical Ltd., [4]Kinki University School of Medicine, [5]National Hosp. Organ. Minami-wakayama Medical Center)

牧 智紀[1‡]、椎名 毅[1]、山川 誠[2]、三竹 毅[3]、工藤 正俊[4]、藤本研治[5]([1]京都大学 医学研究科、[2]京都大学 先端医工学研究ユニット、[3]日立アロカメディカル(株)、[4]近畿大学 医学部消化器内科、[3]南和歌山医療センター)

1. Introduction

Precise evaluation of the stage of chronic hepatitis C with respect to fibrosis has become an important issue to prevent the occurrence of cirrhosis and to initiate appropriate therapeutic intervention. Real-time elastography enables us to evaluate the stiffness of tissue and is a new method for noninvasive staging of liver fibrosis combing of some features from elasticity image. We developed a dynamic model of fibrosis progression in order to quantitatively evaluate the relation between these values and the progression. This paper presents a model and the analysis of an elasticity image based on it.

2. Method

2. 1. Modeling of Fibrosis Progression

The human liver is composed of many hexagonal structures termed liver lobules and containing a central vein. Fibrosis progression is accompanied by changes of tissue structure. When fibrosis grows, the lobules are destroyed and replaced by regenerative nodules.

We can model the liver tissue structure using the potential distribution [1]. With this model, we can monitor and determine the change of liver structure. To prepare the model, we first scattered the central points of the potential distribution corresponding to the central veins and then located the potential distribution around each central point as in eq. (1).

$$p(r) = p_{\max} \sin\left(\frac{\pi}{2} k^{\mathrm{r}}\right) \qquad (1)$$

In eq.(1), $p_{\max}$ is the maximal value and k is the form parameter that determines the distribution defined as the value of 0.8 to 1.2 randomly as an spread. The parameter $p_{\max}$ of all the potentials is initial condition and other parameters are set to experimentally estimated values as discussed in [1].

We simulated the fibrosis progress by combining the potentials and making the nodules and fibers as fibrosis progresses; we assumed that the stage of the model is determined by the number of central points. F0 is the initial state; F1, F2, F3, and F4 are 1/2, 1/4, 1/8, and 1/16 of the initial central number, respectively.

2. 2. Young's modulus distribution

To simulate tissue deformation, values of Young's modulus were assigned to this model composed of parenchyma and fibers. We then assigned Young's modulus [kPa] to the parenchyma based on eq. (2) and allocated it to the fibers based on eq. (3).

$$E_0 = p_{\max} - \bar{p}_{\max,\mathrm{normal}} + E_{\mathrm{normal}} \qquad (2)$$

$$E_1 = 2p_{\max} - \bar{p}_{\max,\mathrm{normal}} + E_{\mathrm{normal}} \qquad (3)$$

In eq.(2) and eq.(3), $\bar{p}_{\max,\mathrm{normal}}$ is the average of the maximal value of each potential for a normal liver model, and E_{normal} is the average Young's modulus on parenchyma of a normal liver model. We established the equations, coefficients, and E_{normal} of 4 [kPa] with reference to practically measured Young's moduli [2].

2. 3. Strain distribution

The tissue deformation caused by compression is simulated by applying the finite element method (FEM) to the tissue model. The Young's modulus distribution model was compressed from upper with pressure of 50kPa (about 1%) and each scatterer

E-mail address: shiina@hs.med.kyoto-u.ac.jp

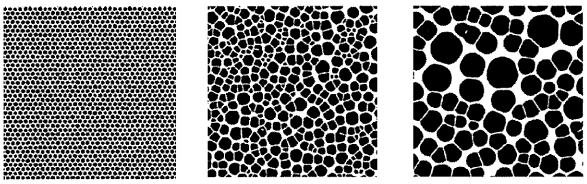

(a)F0 (b)F2 (c)F4

Fig. 1 Change of fibrous structure obtained based on the fibrous progression model.

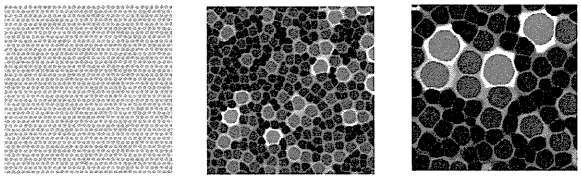

(a)F0 (b)F2 (c)F4

Fig. 2 Young's modulus distribution assigned to deformation model

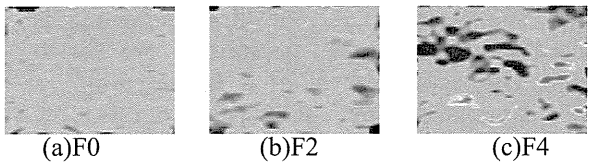

(a)F0 (b)F2 (c)F4

Fig.3 Strain distribution images reconstructed using simulated RF signals

was moved assuming the two-dimensional stress state. Displacement along axial direction was calculated by comparison of two frame data before and after compression. Then, the strain is calculated by differential processing of the displacement.

In addition, strain distribution was obtained by the same way as ultrasound equipment. RF signals were generated from the distribution of scatterers. Then, the strain distribution is calculated by combined autocorrelation method (CAM), which we have developed[3] and applied to ultrasound equipment(the Real-time Tissue Elastography, Hitachi Aloka Medical Ltd). Finally, we created the color images of this strain distribution (**Fig.3**)

3. Results

Figure 1 illustrates the fibrous structure of normal and chronic hepatitis obtained based on the fibrous progression model. Two-dimensional model was applied and 2538 central points were distributed within area (40mmx40mm). The number of iteration does not indicate the physical characteristic of the liver directly, but is selected to only determine the size of nodules. **Fig 1** (a) presents the normal liver, and (b) and (c) depict the liver tissue when fibrosis progresses and the number of the central points has decreased to1/4 and 1/16 compared to the normal state. We can

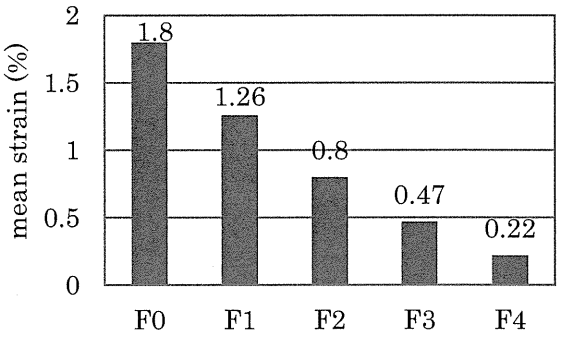

Fig. 4 The relationship between the stage of fibrosis and the mean strain of each stage.

observe that the fiber area increases as the disease progresses.

Figure 2 illustrates the Young's modulus distribution, and Figs. 2 (a) through (c) are Young's moduli assigned to the models in Figs. 1 (a) through (c). As fibrosis progresses, the maximum potential becomes higher, so Young's modulus increases accordingly due to eqs. (2) and (3).

Figures 3 (a) through (c) present strain distribution images obtained by using the CAM. As fibrosis progresses, the blue area increases, indicating that the area has become stiffer than the area around it. In addition, the strain distribution becomes more and more complex. Figure 4 presents the average strain of each stage. We can see that the average strain decreases as the stage progresses.

4. Conclusion

This study proposed a dynamic model of fibrosis progression. From the strain distribution, we could see that the area of low strain increases, the average strain decreases, and the strain distribution becomes more and more complex as fibrosis progresses. These changes are actually seen in elastography. In the future, we will examine the relationship between the models and the clinical data and confirm whether the models are correct. We will then need to establish new staging using a dynamic model so that we can quantitatively diagnose the fibrosis progression.

Acknowledgment

This work was supported by Grant-in-Aid for Science Research[22103507], MEXT, Japan.

References

1.T.Yamaguchi,K.Nakamura,and H.Hachiya :Jpn. J.Appl. Phys.**42** (2003) 3292

2. Clinical Handbook FibroScan(Echosens)

3. M.Yamakawa and T.Shiina : Jpn. J. Appl. Phys. **40** (2001)3872.

The United States of America

The Director of the United States Patent and Trademark Office

Has received an application for a patent for a new and useful invention. The title and description of the invention are enclosed. The requirements of law have been complied with, and it has been determined that a patent on the invention shall be granted under the law.

Therefore, this

United States Patent

Grants to the person(s) having title to this patent the right to exclude others from making, using, offering for sale, or selling the invention throughout the United States of America or importing the invention into the United States of America, and if the invention is a process, of the right to exclude others from using, offering for sale or selling throughout the United States of America, or importing into the United States of America, products made by that process, for the term set forth in 35 U.S.C. 154(a)(2) or (c)(1), subject to the payment of maintenance fees as provided by 35 U.S.C. 41(b). See the Maintenance Fee Notice on the inside of the cover.

David J. Kappos

Director of the United States Patent and Trademark Office

US008041415B2

(12) **United States Patent**
Shiina et al.

(10) **Patent No.: US 8,041,415 B2**
(45) **Date of Patent: Oct. 18, 2011**

(54) **ULTRASONIC DIAGNOSIS SYSTEM AND STRAIN DISTRIBUTION DISPLAY METHOD**

(75) Inventors: **Tsuyoshi Shiina**, Ibaraki (JP); **Makoto Yamakawa**, Ibaraki (JP); **Naotaka Nitta**, Ibaraki (JP)

(73) Assignees: **Tsuyoshi Shiina**, Ibaraki (JP); **Hitachi Medical Corporation**, Tokyo (JP)

(*) Notice: Subject to any disclaimer, the term of this patent is extended or adjusted under 35 U.S.C. 154(b) by 1830 days.

(21) Appl. No.: **10/522,807**

(22) PCT Filed: **Jul. 31, 2003**

(86) PCT No.: **PCT/JP03/09731**
§ 371 (c)(1),
(2), (4) Date: **Jan. 31, 2005**

(87) PCT Pub. No.: **WO2004/010872**
PCT Pub. Date: **Feb. 5, 2004**

(65) **Prior Publication Data**

US 2006/0052696 A1 Mar. 9, 2006

(30) **Foreign Application Priority Data**

Jul. 31, 2002 (JP) 2002-222868
Jul. 31, 2002 (JP) 2002-222869

(51) **Int. Cl.**
A61B 8/00 (2006.01)

(52) **U.S. Cl.** **600/433**; 600/437; 600/442; 600/463

(58) **Field of Classification Search** 600/437–447, 600/450; 73/787
See application file for complete search history.

(56) **References Cited**

U.S. PATENT DOCUMENTS

5,462,058	A	10/1995	Yamada	
5,524,636	A *	6/1996	Sarvazyan et al.	600/587
6,277,074	B1	8/2001	Chaturvedi	
7,223,241	B2 *	5/2007	Radulescu	600/443

(Continued)

FOREIGN PATENT DOCUMENTS

DE 198 24 108 12/1999

(Continued)

OTHER PUBLICATIONS

Tsuyoshi Shiina, et al. "Real Time Tissue Elasticity Imaging Using the Combined Autocorrelation Method", J Med Ultrasonics, vol. 26, No. 2 (1999), pp. 57-66.

(Continued)

Primary Examiner — Unsu Jung
Assistant Examiner — Lawrence N Laryea
(74) *Attorney, Agent, or Firm* — Antonelli, Terry, Stout & Kraus, LLP.

(57) **ABSTRACT**

An ultrasonic diagnosis system and strain distribution display method utilizing an ultrasonic probe for performing transmission/reception of ultrasonic signals to/from a subject, a storage arrangement for storing the properties of signals detected with the ultrasonic probe, a correlation computer for calculating a correlation coefficient between the properties with and without pressure applied to the subject, and a phase difference between the received signals with and without application of pressure, based upon the properties stored in the storage arrangement with and without pressure applied to the subject, a computer for calculating a displacement of each measurement point, and a strain distribution of tissue of the subject due to application of pressure, based upon the correlation coefficient and phase difference calculated by the correlation computer, and a display for displaying the strain distribution.

30 Claims, 25 Drawing Sheets